Kinetic-oriented construction of MoS_2 synergistic interface to boost pH-universal hydrogen evolution

Jue Hu,[1,+] Chengxu Zhang,[2,+] Peng Yang,[1] Mingzi Sun,[3] Jingyi Xiao,[4] Tao Deng,[1] Zhiyong Liu,[1] Bolong Huang,[3,*] Michael K. H. Leung,[4,*] and Shihe Yang[5,*]

Prof. J. Hu, P. Yang, T. Deng, Z. Liu
Faculty of Science, Kunming University of Science and Technology, Kunming, 650093, China.

C. Zhang
The Engineering Laboratory of Advanced Battery and Materials of Yunnan Province, Faculty of Metallurgical and Energy Engineering, Kunming University of Science and Technology, Kunming, 650093, China.

M. Sun and Prof. B. Huang
Department of Applied Biology and Chemical Technology, The Hong Kong Polytechnic University, Hung Hom, Kowloon, Hong Kong SAR, 999077, China.
Email: bhuang@polyu.edu.hk

J. Xiao and Prof. K. H. Leung
Ability R&D Energy Research Centre, School of Energy and Environment, City University of Hong Kong, Hong Kong, 999077, China.
Email: mkh.leung@cityu.edu.hk

Prof. S. Yang
Guangdong Key Lab of Nano-Micro Material Research, School of Chemical Biology and Biotechnology, Shenzhen Graduate School, Peking University, Shenzhen 518055, China
Email: chsyang@ust.hk

Keywords: MoS_2, Interfacial Electrocatalysis, Kinetic Oriented Mechanism, Hydrogen Evolution, pH-universal

As a prerequisite for future sustainable energy economy, designing earth-abundant MoS_2 catalysts with comparable hydrogen evolution catalytic performance in both acidic and alkaline environment is still an urgent challenge. Decreasing the energy barriers could enhance the catalysts' activity but is not often a strategy for doing so. Here, we present the first kinetics-oriented design of the MoS_2 based heterostructure for pH-universal hydrogen evolution catalysis by optimizing the electronic structure based on the simultaneous modulation of the 3d-band-offsets of Ni, Co and Mo near the interface. Benefiting from this desirable electronic structure, the obtained $MoS_2/CoNi_2S_4$ catalyst achieves an ultralow overpotential of 78 mV and 81 mV at 10 mA/cm^2, and turnover frequency as high as 2.7 s^{-1} and 1.7 s^{-1} at the overpotential of 200 mV in alkaline and acidic media, respectively. The $MoS_2/CoNi_2S_4$ catalyst represents

one of the best HER performing ones among the MoS_2-based catalysts reported to date in both alkaline and acidic environments, and equally important is remarkable long-term stability with negligible activity loss after maintaining at 10 mA/cm^2 for 48h in both acid and base. This work highlights the potential to deeply understand and rationally design highly efficient pH-universal electrocatalysts for future energy storage and delivery.

Establishing a global-scale sustainable hydrogen energy system to solve the global energy crisis, climate change, and environmental problems is a pivotal challenge for the whole society nowadays [1]. The electrocatalytic water-splitting reaction is emerging as the most attractive green technology for affording hydrogen and oxygen by hydrogen evolution reactions (HER) and oxygen evolution reaction (OER), where the electrocatalysts are vital in guaranteeing the energy conversion[2]. Indeed, platinum is the best performing catalyst for HER, their broad application in large-scale hydrogen generation is still constrained by the high cost and low earth-abundance issues. Earth-abundant catalysts, especially transition metal chalcogenides, carbides, nitrides, and phosphides have been wildly explored in recent decades and some of them indeed show satisfied HER catalytic performance[3]. Among them, molybdenum disulfide (MoS_2) has emerged as a promising non-precious-metal HER electrocatalyst in acidic enviorment[4]. Furthermore, great efforts have been devoted to building heterostructure catalysts to facilitate the rate-determining water dissociation steps for the hydrogen evolution catalysis in alkaline media[5]. However, few of these electrocatalysts exhibit competitive HER catalytic performance in base as that in acid, even fewer show the pH-universal activity and stability. Thus, developing the advanced earth-abundant electrocatalysts with enhanced HER catalytic performance in both acidic and alkaline environment is an urgent issue.

At present, there is still no direct evidence for the mechanism responsible for the puzzling difference of HER catalytic activity between in acid and base, let alone optimizing the HER

catalytic performance based on such mechanism.[6] Beyond the limited ability to modulate catalytic properties of the currently reported catalysts with random building heterostructure, the kinetics-oriented construction of the well-designed interfacial composite catalysts will be a potential new strategy that may maximize and multiply the advantages of heterostructure catalysts towards the HER.

For HER, the formation of adsorbed hydrogen (H_{ad}) largely depends on the electronic interactions with the catalyst surface which dictates the thermodynamics and kinetics of the hydrogen evolution catalysis.[2] Regarding the promising noble-metal-free MoS_2 catalyst, the kinetic analysis indicates much higher reaction barriers of the Tafel step than that of the Heyrovsky step for HER in both acidic and alkaline electrolytes, suggesting the Volmer-Heyrovsky pathway as the dominant HER mechanism on the MoS_2 surface (**Supplementary Note 1** and **Figure S1**).[6a, 7] Furthermore, the reaction barriers of the dominant Volmer and Heyrovsky steps in alkaline media are much higher than those in acidic one based on the kinetics analysis, leading to the inferior HER performance of MoS_2 catalyst in alkaline media **(Figure 1a, b** and **Figure S2-4**). Our previous work demonstrated that the hybridization of MoS_2 and layered double hydroxide (LDH) materials, which synergistically favored the adsorption of intermediates (H and OH) near the interfaces, accelerating both the Volmer and Heyrovsky steps of HER, and as a result, the overall HER kinetics in base will be significantly improved.[8] Unfortunately, the HER kinetics becomes more sluggish in acidic media on the MoS_2/NiCo-LDH surface because of the largely increased standard free energy of intermediate adsorption ($\Delta G_{\mathrm{ad}}^{0}$), which reflects a weakened binding of the intermediates **(Figure 1b**) and as a result the higher energy barriers of the rate-determining Volmer and Heyrovsky steps in acid than those in base, leaving the search for catalysts with fast kinetics in both acid and base as a huge challenge in the HER research.[6a] The key to such a goal will be the well-balanced intermediates bonding and releasing abilities on the catalyst surface to decrease the energy

barriers of the dominant Volmer and Heyrovsky steps. As has been demonstrated, both the active edged sites and the inert basal plane on MoS_2 surfaces tend to bond H_{ad} weakly,[9] thereby accelerating the kinetics of the rate-determining Volmer and Heyrovsky steps should facilitate the intermediates adsorption. Indeed, **Figure 1a** reveals that the standard activation free energies for Volmer step (ΔG_{-V}^{*0}) and Heyrovsky step (ΔG_{+H}^{*0}) have positive correlation with the standard free energy of adsorption for the reaction intermediate (ΔG_{ad}^{0}) on the MoS_2 and MoS_2/NiCo-LDH surfaces, indicating that the intermediates adsorption capability plays a key role in tuning the HER kinetics on the earth-abundant MoS_2 surfaces. Herein, we document the synergistic $MoS_2/CoNi_2S_4$ heterostructure catalyst in actualizing the exceptional pH-universal HER performance for the first time. Through the rational theory design and synthesis, the obtained $MoS_2/CoNi_2S_4$ catalyst with remarkable activity has achieved the ultra-low overpotentials as 78 mV and 81 mV at 10 mA/cm^2 in alkaline and acidic media, respectively, which are superior to those of most newly reported highly active pH-universal catalysts. The kinetic investigations with theoretical calculations reflect the interfacial activation of the optimal electronic distribution on $MoS_2/CoNi_2S_4$ will lead to the substantial energetic benefit for efficient HER in a universal environment.

Design of $MoS_2/CoNi_2S_4$. Our kinetics analysis suggests that the kinetically favorable HER catalysts should possess facilitated intermediates adsorption capability for efficient Volmer and Heyrovsky steps and optimal adsorption energy of H_{ad} to balance the under-binding and over-binding effect. In this light, it is instructive to build the $MoS_2/CoNi_2S_4$ composite, which possesses a heterostructure for efficient both H and OH intermediates adsorption and optimal electronic structure for modulating the binding strength of H_{ad}. We further applied the density function theory (DFT) to analyze the electronic structure. The local structure of the electronically active interface (IF) is constructed by the close connection between MoS_2(002) and $CoNi_2S_4$(400) (**Figure 1b**). The strain has induced evident distortion of the structure that

leads to surface reconstruction, especially in the IF region. The uniform distribution of bonding and anti-bonding orbitals near the Fermi level (E_F) endows the surface a good charge transfer capability. To gain more insight into the origin of the electroactivity, we further interpret the electronic contributions to different regions in $MoS_2/CoNi_2S_4$. We find the evolution of the projected partial density of states (PDOS) from Mo in the $MoS_2/CoNi_2S_4$ displays a feature in a very broad range from -6 eV below E_F to across the E_F, which is similar with the PDOS of the metal phase (**Figure 1c**). In contrast to the pristine MoS_2 bulk, the introduction of $CoNi_2S_4$ also largely attenuated the gap between e_g and t_{2g} of Mo-4d. Such high electronic activities will not only contribute to the HER process but also exhibit as a wide-range modulator to boost the inter-sites electron transfer based on activation of the local electronic structures of Ni and Co from $CoNi_2S_4$.

Interestingly, an optimal local electronic structure is achieved via the simultaneously converse modification of 3d bands of Ni and Co. The relatively less active Ni near IF has been activated by the electronic modulation from Mo (**Fig. 1d**). As getting closer to the IF region, the Ni-3d bands monotonically migrating from deep localization positions (E_F-2.25 eV) to the high-lying position with a positive band offset around 1.25 eV, indicating an optimized under-binding effect induced by Ni in the IF region of $MoS_2/CoNi_2S_4$. On the contrary, the PDOS of Co in bulk $CoNi_2S_4$ is staying at a higher position near E_F, however, its position in $MoS_2/CoNi_2S_4$ has been gradually suppressed to a lower position towards the IF region with a 1.25 eV negative band offset (**Fig. 1e**). This suppression will optimize the over-binding effect induced by Co for better efficiency of H_2 generation. The DFT calculations unraveled an evident modification to the Ni and Co concurrently by the electronic modulator Mo, which not only activates the Ni but also balances the over-binding effect from Co. The optimized interfacial electronic properties guarantee the desired high HER performance in both the acidic and alkaline environment.

Synthesis and structural characterization of $MoS_2/CoNi_2S_4$. Guided by the design strategy and the theoretical calculations, the $MoS_2/CoNi_2S_4$ composite was fabricated using a two-step hydrothermal process. In our experiment, Co-Ni hydroxides nanowires were directly grown on carbon fiber paper substrate as the precursor (**Figure S5**). Then, $MoS_2/CoNi_2S_4$ composite was synthesized by simultaneous sulfurization of Co-Ni hydroxide precursor and generation of MoS_2 (see **Supporting Information** for details). As control samples, bare MoS_2, $CoNi_2S_4$, and MoS_2/NiS_2, MoS_2/Co_3S_4 composites were prepared by a similar procedure (**Figure S6-8**). The microstructure of $MoS_2/CoNi_2S_4$ composite was directly imaged by field-emission scanning electron microscopy (FESEM). The FESEM images of $MoS_2/CoNi_2S_4$ show MoS_2 nanosheets fabricated microrods are uniformly covered with a smooth surface as illustrated in the inset picture of **Figure 2a** (**Figure 2a** and **Figure S9**). This similar covered morphology can be also seen for the MoS_2/NiS_2 and MoS_2/Co_3S_4 composites as shown in **Figure S10**. Elemental mappings evidence the uniform distribution of Mo, Co, Ni and S on the $MoS_2/CoNi_2S_4$ surface (**Figure S11**). The transmission electron microscopy (TEM) images show that the $CoNi_2S_4$ is mainly covered on the edges of MoS_2 nanosheets as illustrated in **Figure 1a** and **Figure S12**. The good covering of $CoNi_2S_4$ onto MoS_2 nanosheets suggests not only plenty electrocatalytic active sites on the surface but also a potential interfacial reaction, which would benefit long-term durability.

Further high-resolution transmission electron microscopy (HRTEM), X-ray diffraction (XRD) and X-ray photoelectron spectroscopy (XPS) analyses manifest the heterostructure nature of the $MoS_2/CoNi_2S_4$ composite. In **Figure 2b**, HRTEM image of $MoS_2/CoNi_2S_4$ shows a clear heterojunction between the MoS_2 (002) and $CoNi_2S_4$ (400) phases. The fast Fourier transformation (FFT) pattern in area i marked by the white dashed square in the HRTEM image, shows clear reflections of (220), (440), (400) facets of $CoNi_2S_4$ crystallites, which is consistent with the FFT pattern of the pure $CoNi_2S_4$ crystallites as shown in **Figure S13**. In the dark dashed

marked area ii of **Figure 2b**, the FFT pattern reflects the (220), (440), (400) facets of $CoNi_2S_4$ as well as the (002) and (110) facets of MoS_2, confirming the interface construction between MoS_2 and $CoNi_2S_4$. The heterostructure of the $MoS_2/CoNi_2S_4$, MoS_2/NiS_2 and MoS_2/Co_3S_4 composites is further justifying by XRD (**Figure 2c** and **Figure S14-15**). All diffraction peaks of the $MoS_2/CoNi_2S_4$ composite sample match well with the corresponding standard patterns of 2H-MoS_2 and $CoNi_2S_4$ (JCPDS No. 75-1539 and 24-0334, respectively) and are well consistent with the FFT patterns. The Mo 3d, Ni 2p and Co 2p XPS spectra in **Figure 2d-f** and **Figure S14-15.** reveal the chemical compositions and surface electronic states of these elements in the $MoS_2/CoNi_2S_4$, MoS_2/NiS_2 and MoS_2/Co_3S_4 composite samples. Peak deconvolutions were carried out to fit these spectra. The typical Mo^{4+} peaks are located at 228.9 eV and 232.1 eV for Mo $3d_{5/2}$ and $3d_{3/2}$, respectively. Peaks with higher energies for Mo^{6+} $3d_{5/2}$ at 232.8 eV and MoO_{3-x} $3d_{5/2}$ at 230.7 eV are also observed in the $MoS_2/CoNi_2S_4$ sample (**Figure 2d**)[10]. In addition, the Ni 2p and Co 2p XPS spectra (**Figure 2e-f**) reveal the oxidation states of Ni^{2+}, Ni^{3+} for Ni element and Co^{2+} and Co^{3+} for Co element are mainly exist in the $MoS_2/CoNi_2S_4$ composite with the Ni/Co ratio of 2.28:1. There are slight shifts of the binding energies for Mo 3d in $MoS_2/CoNi_2S_4$ comparing with the pure MoS_2, and for both Ni 2p, Co 2p in $MoS_2/CoNi_2S_4$ comparing with the pure $CoNi_2S_4$ sample, providing important evidence for the electronic interactions between MoS_2 and $CoNi_2S_4$ (**Figure S16**)[8].

The HER catalytic behavior. We examined the HER catalytic behavior of the $MoS_2/CoNi_2S_4$, MoS_2/NiS_2 and MoS_2/Co_3S_4 composite catalysts with the representative linear sweep voltammograms (LSVs) in both alkaline and acidic electrolytes summarized in **Figure 3a,d**. For comparison, the bare MoS_2, $CoNi_2S_4$, NiS_2, Co_3S_4, and commercial Pt/C catalysts were also studied under the same conditions. In H_2 saturated 1 M KOH solution, the MoS_2/metal sulfide composites show much decreased overpotential and significantly improved current density, indicating the HER electrocatalytic performance of the $MoS_2/CoNi_2S_4$, MoS_2/NiS_2 and

MoS_2/Co_3S_4 composite catalysts are substantially better than those of the bare MoS_2, $CoNi_2S_4$, NiS_2, Co_3S_4 catalysts, and even better than the commercial Pt/C catalyst at high current density range. Among them, $MoS_2/CoNi_2S_4$ exhibits the best HER electrocatalytic activity with the smallest overpotential of 78 mV at 10 mA/cm^2 and the highest catalytic current density across the entire potential range, which is superior to the overpotential of 111 mV for MoS_2/NiS_2 and 152 mV for MoS_2/Co_3S_4, revealing the pivotal effect of electronic structure modulation of electrocatalytic active sites. The Tafel slope of $MoS_2/CoNi_2S_4$ is measured as 67 mV/dec, which is much smaller than the bare MoS_2 (95 mV/dec) and $CoNi_2S_4$ (145 mV/dec) catalysts, indicating superior HER kinetics for $MoS_2/CoNi_2S_4$ (**Figure 3b**). In addition, the Tafel slopes for $MoS_2/CoNi_2S_4$, MoS_2/NiS_2 and MoS_2/Co_3S_4 composite catalysts are all within the range of 39 to 116 mV/dec, suggesting the rate-determining step of the hydrogen evolution catalysis is the charge-transfer-induced water dissociation step on these catalysts surfaces, where the Volmer step and Heyrovsky step are kinetically comparable[8].

The hydrogen evolution catalysis behavior was further investigated by electrochemical impedance spectroscopy (EIS). The EIS results further justify the exceptional HER kinetics of $MoS_2/CoNi_2S_4$, where the Nyquist plots (**Figure S17**) show the smallest charge transfer resistance for $MoS_2/CoNi_2S_4$ among the tested catalysts at the overpotential of 200 mV, indicating the superior interfacial charge-transfer kinetics. To access the intrinsic activity of the $MoS_2/CoNi_2S_4$, MoS_2/NiS_2 and MoS_2/Co_3S_4 composite catalysts, it is vital to eliminate the contribution derived from the electro chemically active surface area (ECSA) and calculate the turnover frequency (TOF). As shown in **Figure S17-20**, the double-layer capacitance (C_{dl}), which is expected to evaluate the ECSA for transition metal compounds[11], of $MoS_2/CoNi_2S_4$ (122.1 mF/cm^2) is close to that of bare MoS_2 (123.3 mF/cm^2), indicating that the enhancement does not originate from the ECSA but the introduction of $CoNi_2S_4$ onto MoS_2 surface which intrinsically changes the hydrogen evolution catalysis. Assuming that all the Mo sites were

electrochemically active in the HER process[8, 12], the calculated turnover frequency (TOF) for $MoS_2/CoNi_2S_4$ composite reaches 2.7 s^{-1}, which is 13 times higher than that of MoS_2 (0.2 s^{-1}) at the overpotential of 200 mV (**Figure 3c**), demonstrating the synergistic catalytic effect manifest on the $MoS_2/CoNi_2S_4$ heterostructure.

In H_2 saturated 0.5 M H_2SO_4 solution, the bare MoS_2 exhibits an overpotential of 166 mV at 10 mA/cm^2 and Tafel slope of 75 mV/dec, being close to those reported values for hydrothermal synthesized MoS_2 in the literature (**Figure 3c.d**)[13]. It is noted that the HER catalytic activity of MoS_2 is significantly improved after fabricating the heterostructure. With $MoS_2/CoNi_2S_4$, the HER activity is boosted with the overpotential as low as 81 mV at 10 mA/cm^2. The Tafel slopes of the tested catalysts are within the range of 39 to 116 mV/dec. The TOF for $MoS_2/CoNi_2S_4$ composite is 1.7 s^{-1} at the overpotential of 200 mV in acid (**Figure S21**). **Figure S22-23** and **Supplementary Table 1-2** summarized the overpotentials at 10 mA/cm^2 and Tafel slopes for the most active molybdenum, nickel and cobalt-based compound catalysts in base and acid, respectively. Obviously, these energetic metrics for $MoS_2/CoNi_2S_4$ composite outperform or at least comparable to those of the most active HER electrocatalysts in alkaline or acidic electrolytes, making our $MoS_2/CoNi_2S_4$ composite a superior catalyst to most previously reported noble-metal-free HER catalysts. Furthermore, the $MoS_2/CoNi_2S_4$ composite exhibits the lowest overpotentials in both acidic and alkaline electrolytes (81 mV in 0.5 M H_2SO_4 and 78 mV in 1 M KOH at 10 mA/cm^2) among the tested catalysts, which are even markedly lower than those of most newly reported highly active pH-universal catalysts, suggesting that the HER electrocatalytic performance of $MoS_2/CoNi_2S_4$ composite is among the best range for the noble-metal-free pH-universal catalysts (**Figure 3f** and **Supplementary Table 3**)[14].

We combined the electrochemical measurements to verify the electrocatalytic durability of our $MoS_2/CoNi_2S_4$ catalyst. During the chronopotentiometry measurement, the overpotential of Pt/C catalyst increases more than 150 mV at 10 mA/cm^2 for 48 h in the alkaline electrolyte and 15 mV 10 mA/cm^2 for 18 h in the acidic electrolyte (**Figure 4 a.b**). Interesting, the chronopotentiometry measurement results manifest that the synthesized $MoS_2/CoNi_2S_4$ catalyst exhibits an outstanding long-term operational durability for 48 h at 10 mA/cm^2 with no observed overpotential increase in both 1 M KOH and 0.5 M H_2SO_4 electrolytes. In addition, there is no difference in the ECSA of after 48 h at 10 mA/cm^2 (**Figure S24**). Moreover, the HER catalytic performance of $MoS_2/CoNi_2S_4$ catalyst shows no obvious difference between initial and after the long-term durability test, indicating the striking electrocatalytic durability of the $MoS_2/CoNi_2S_4$ catalyst in both alkaline and acidic media. We further examined the $MoS_2/CoNi_2S_4$ catalyst using XPS characterization after the chronopotentiometry test in 1 M KOH at 10 mA/cm^2 for 48 hours (**Figure 4c-f**). The high-resolution Ni 2p and Co 2p spectra of $MoS_2/CoNi_2S_4$ composite manifest that the concentration of the higher valence component of Ni (Ni^{3+}) decreases after the durability test, while that of the higher valence component of Co (Co^{3+}) increases, revealing the inter-sites electron transfer and charge redistribution on the surface. Interestingly, the doublet peaks of Mo^{6+} decrease and the doublet peaks of MoO_{3-X} disappear after the durability test, while the intensities of the doublet peaks for Mo^{4+} increase, which may be induced by similar electron transfer via interfacial chemical bonds. Regarding the S 2p spectra, it is obvious that there is no difference in S components of the $MoS_2/CoNi_2S_4$ composite after 48-hours durability measurement. The excellent HER electrocatalytic activity and long-term durability of the $MoS_2/CoNi_2S_4$ composite suggest the great promise to serving as pH-universal platinum-like electrocatalyst for HER.

The dual-pathway kinetic analyses and DFT calculations have been carried out for the insightful understanding of the enhanced HER performance of $MoS_2/CoNi_2S_4$ composite in the pH-

universal environment. Following the procedure of Wang *et al*. and our previous work[6a, 7-8], we performed kinetic analyses by well-fitting the kinetic current density of $MoS_2/CoNi_2S_4$ composite to evaluate the standard activation free energies for the three elementary reaction steps (Volmer, Heyrovsky and Tafel steps) of HER in both acidic and alkaline media (**Figure 5a**). The fractional coverages (θ) of the active reaction intermediate, H_{ad}, on the $MoS_2/CoNi_2S_4$ surface in acid and base are similar and within a high level, indicating the high intrinsic activity of the active sites. The free energy diagrams indicate a dominant Volmer-Heyrovsky (V-H) pathway of HER on $MoS_2/CoNi_2S_4$ surface in both acid and base, where the activation energy of Heyrovsky step is much lower than that of Tafel step, which is in good agreement with the Tafel slope analysis (**Figure 5b** and **Figure S25**). The relatively low values of ΔG_{ad}^{0} in both acid and base indicate an efficient adsorption of the intermediates on the $MoS_2/CoNi_2S_4$ surface, and as a result accelerating Volmer and Heyrovsky steps in both acid and base. Indeed, in acidic environment, the activation energies of $MoS_2/CoNi_2S_4$ for both Heyrovsky and Volmer steps are slightly lower than those of our previously reported stepped edged terminated MoS_2 nanosheet array, indicating even better HER kinetics of $MoS_2/CoNi_2S_4$ than se-MoS_2 in acid. Furthermore, the activation energies of $MoS_2/CoNi_2S_4$ for both Heyrovsky and Volmer steps in an alkaline environment are much lower than those of se-MoS_2, justifying that the hybridization of MoS_2 with $CoNi_2S_4$ accelerates the charge-transfer-induced water dissociation steps of HER in the alkaline environment.

Based on the DFT calculations, the compensated modification of the 3d bands between Ni and Co illustrates a charge redistribution on the surface that significantly optimizes the electronic environment for the HER that achieve the preferred balance between reactivity and over-binding effect of the surface. Thus, the optimized electronic structure of Ni promotes the adsorption of H_2O near IF region for the HER in the alkaline environment. The optimal adsorption position of the H atom and H_2O for both HER in acid and alkaline environment also

demonstrate a high electronic activity near the IF region (**Figure 5c**). The 3d bands of Ni mainly locate from E_F-6 eV below E_F+2 eV that widely matched with the *s,p* bands of H_2O, illustrating the stable adsorption with active charge exchange between the Ni and adsorbed H_2O (**Figure 5d**). Moreover, the well overlap between Ni-3d and H_2O-2p between E_F-7 eV and E_F- 1 eV representing a strong Ni-O σ-bonding, which will reduce the binding strength of O-H for easier dissociation of H_2O in alkaline HER. Accordingly, the IF Ni-sites will perform the best initial water adsorption and the following smooth desorption of OH will be ensured due to the limited overlap between Ni-3d and O-2p near E_F. Therefore, the efficient HER process without over-binding effect will be expected based on the optimal electronic distribution near the IF region in $MoS_2/CoNi_2S_4$. Meanwhile, the HER process in the alkaline process also demonstrates a continuous downhill reaction trend with energy releasement of -1.08 eV (**Figure 5e**), illustrating an energetically favorable pathway for HER. The adsorption of H_2O near IF-Ni site and the adsorption of H near the IF-Mo region will lead to the close-contacted H-adsorption for the following efficient H_2 generations (**Figure 5c**). The barriers of transition states in the alkaline HER process are around the scale of 0.3 eV, which will be overcome with the assistance of the local distorted structures. We further analyze the universal reactivity of $MoS_2/CoNi_2S_4$ from an energetic perspective regarding the H-formation comparison and free energy pathway. The formation energy which is related the adsorption of the H and H_2 species is consistent with the electronic properties (**Figure 5f**). All the adsorptions near-neutral adsorption line (E = 0 eV) are located near the IF region. The chemisorption of H is reasonable that will not result in the over-binding. The HER process in the acidic environment from $2H^* \rightarrow H_2$ are energetically favorable in downhill trend with the nearly negligible energy barrier. Therefore, these results confirmed that the $MoS_2/CoNi_2S_4$ could serve as a superior pH-universal electrocatalyst for HER.

In summary, we have presented the kinetics-orientedly designed $MoS_2/CoNi_2S_4$ composite for the first time as a low-cost, highly efficient and stable catalyst for the HER over a wide pH range based on theory-calculation guidance and rational experimental design. DFT analysis unravels an evident modification to the Ni and Co concurrently by the electronic modulator Mo in $MoS_2/CoNi_2S_4$, which not only activates the Ni but also alleviate the over-binding effect from Co. Leveraging on the desirable electronic structure, the $MoS_2/CoNi_2S_4$ composite catalyst guarantee the efficient H and OH adsorption in alkaline environment as well as the optimal binding strength of H_{ad} in acidic media, supporting the outstanding HER electrocatalytic activity and long-term stability as a pH-universal electrocatalyst. The remarkable energetic HER kinetics is further justified by the dual-pathway kinetic analysis and the outstanding electrochemical performance with ultra-low overpotential and high TOF value, which outperformed most recently reported pH-universal electrocatalyst. Our study demonstrates the rational interfacial design strategy to promote the pH-universal HER process that is applicable to a broad class of MoS_2-based electrocatalysts. This work will open a new direction in developing potential earth-abundant catalysts with competitive performance.

Supporting Information
Supporting Information is available from the Wiley Online Library or from the author.

Acknowledgements
This research is supported by National Nature Science Foundation of China (Nos. 21862011, 51864024), the Kunming University of Science and Technology (Nos. KKKP201707010, KKKP201752011), the Shenzhen Pea-cock Plan (KQTD2016053015544057), the Nanshan Pilot Plan (LHTD20170001) and the Guangdong Science and Technology Program (2017B030314002).

Received: ((will be filled in by the editorial staff))
Revised: ((will be filled in by the editorial staff))
Published online: ((will be filled in by the editorial staff))

References

[1] Z. W. Seh, J. Kibsgaard, C. F. Dickens, I. Chorkendorff, J. K. Nørskov, T. F. Jaramillo, *Science* **2017**, *355*, eaad4998.
[2] D. Voiry, H. S. Shin, K. P. Loh, M. Chhowalla, *Nature Rev. Chem.* **2018**, *2*, 0105.
[3] a) X. Huang, Z. Zeng, H. Zhang, *Chem. Soc. Rev.* **2013**, *42*, 1934-1946; b) X. Zou, Y. Zhang, *Chem. Soc. Rev.* **2015**, *44*, 5148-5180; cY. M. Shi, B. Zhang, *Chem. Soc. Rev.* **2016**, *45*, 1529-1541; d) X. Y. Chia, A. Y. S. Eng, A. Ambrosi, S. M. Tan, M. Pumera, *Chem. Rev.* **2015**, *115*, 11941-11966; e) J. Hu, C. Zhang, X. Meng, H. Lin, C. Hu, X. Long, S. Yang, *J. Mater. Chem. A* **2017**, *5*, 5995-6012; f) I. K. Mishra, H. Zhou, J. Sun, F. Qin, K. Dahal, J. Bao, S. Chen, Z. Ren, *Energy Environ. Sci.* **2018**, *11*, 2246-2252; gZ. Pu, J. Zhao, I. S. Amiinu, W. Li, M. Wang, D. He, S. Mu, *Energy Environ. Sci.* **2019**, *12*, 952-957.
[4] a) H. T. Wang, Z. Y. Lu, S. C. Xu, D. S. Kong, J. J. Cha, G. Y. Zheng, P. C. Hsu, K. Yan, D. Bradshaw, F. B. Prinz, Y. Cui, *P. Natl. Acad. Sci. USA* **2013**, *110*, 19701-19706; b) J. Wang, M. Yan, K. Zhao, X. Liao, P. Wang, X. Pan, W. Yang, L. Mai, *Adv. Mater.* **2017**, *29*, 1604464-n/a; c) Q. Ding, B. Song, P. Xu, S. Jin, *Chem* **2016**, *1*, 699-726; d) Y. Yin, J. Han, Y. Zhang, X. Zhang, P. Xu, Q. Yuan, L. Samad, X. Wang, Y. Wang, Z. Zhang, P. Zhang, X. Cao, B. Song, S. Jin, *J. Am. Chem. Soc.* **2016**, *138*, 7965-7972; e) G. Zhang, H. J. Liu, J. H. Qu, J. H. Li, *Energy Environ. Sci.* **2016**, *9*, 1190-1209.
[5] a) R. Subbaraman, D. Tripkovic, D. Strmcnik, K.-C. Chang, M. Uchimura, A. P. Paulikas, V. Stamenkovic, N. M. Markovic, *Science* **2011**, *334*, 1256-1260; b) N. Danilovic, R. Subbaraman, D. Strmcnik, K.-C. Chang, A. P. Paulikas, V. R. Stamenkovic, N. M. Markovic, *Angew. Chem.* **2012**, *124*, 12663-12666; c) M. T. M. Koper, *Nat. Chem.* **2013**, *5*, 255-256; d) P. Wang, X. Zhang, J. Zhang, S. Wan, S. Guo, G. Lu, J. Yao, X. Huang, *Nat. Comm.* **2017**, *8*, 14580.
[6] a) J. X. Wang, T. E. Springer, R. R. Adzic, *J. Electrochem. Soc* **2006**, *153*, A1732-A1740; b) Y.-C. Hsieh, Y. Zhang, D. Su, V. Volkov, R. Si, L. Wu, Y. Zhu, W. An, P. Liu, P. He, S. Ye, R. R. Adzic, J. X. Wang, *Nat. Commun.* **2013**, *4*, 1-9; c) R. Subbaraman, D. Tripkovic, K.-C. Chang, D. Strmcnik, A. P. Paulikas, P. Hirunsit, M. Chan, J. Greeley, V. Stamenkovic, N. M. Markovic, *Nat. Mater.* **2012**, *11*, 550-557; d) J. Durst, C. Simon, F. Hasché, H. A. Gasteiger, *J. Electrochem. Soc* **2015**, *162*, F190-F203; e) J. Hu, K. A. Kuttiyiel, K. Sasaki, C. Zhang, R. R. Adzic, *J. Electrochem. Soc.* **2018**, *165*, J3355-J3362.
[7] a) K. Elbert, J. Hu, Z. Ma, Y. Zhang, G. Chen, W. An, P. Liu, H. S. Isaacs, R. R. Adzic, J. X. Wang, *ACS Catal.* **2015**, *5*, 6764-6772; b) J. X. Wang, T. E. Springer, P. Liu, M. Shao, R. R. Adzic, *J. Phys. Chem. C* **2007**, *111*, 12425-12433.
[8] J. Hu, C. Zhang, L. Jiang, H. Lin, Y. An, D. Zhou, M. K. H. Leung, S. Yang, *Joule* **2017**, *1*, 383-393.
[9] B. Hinnemann, P. G. Moses, J. Bonde, K. P. Jørgensen, J. H. Nielsen, S. Horch, I. Chorkendorff, J. K. Nørskov, *J. Am. Chem. Soc.* **2005**, *127*, 5308-5309.
[10] a) J. Hu, B. Huang, C. Zhang, Z. Wang, Y. An, D. Zhou, H. Lin, M. K. H. Leung, S. Yang, *Energy Environ. Sci.* **2017**, *10*, 593-603; b) D. R. Cummins, U. Martinez, A. Sherehiy, R. Kappera, A. Martinez-Garcia, R. K. Schulze, J. Jasinski, J. Zhang, R. K. Gupta, J. Lou, M. Chhowalla, G. Sumanasekera, A. D. Mohite, M. K. Sunkara, G. Gupta, *Nat. Commun.* **2016**, *7*, 11857.
[11] C. C. L. McCrory, S. Jung, I. M. Ferrer, S. M. Chatman, J. C. Peters, T. F. Jaramillo, *J. Am. Chem. Soc.* **2015**, *137*, 4347-4357.
[12] J. Kibsgaard, T. F. Jaramillo, F. Besenbacher, *Nat. Chem.* **2014**, *6*, 248-253.
[13] C. Zhang, L. Jiang, Y. Zhang, J. Hu, M. K. H. Leung, *J. Catal.* **2018**, *361*, 384-392.
[14] a) H. Yan, Y. Xie, Y. Jiao, A. Wu, C. Tian, X. Zhang, L. Wang, H. Fu, *Adv. Mater.* **2018**, *30*, 1704156; b) Y.-Y. Ma, C.-X. Wu, X.-J. Feng, H.-Q. Tan, L.-K. Yan, Y. Liu, Z.-H. Kang, E.-B. Wang, Y.-G. Li, *Energy Environ. Sci.* **2017**, *10*, 788-798; c) H. Zhang,

P. An, W. Zhou, B. Y. Guan, P. Zhang, J. Dong, X. W. Lou, *Sci. Adv.* **2018**, *4*, eaao6657; d) F. Yang, Y. Chen, G. Cheng, S. Chen, W. Luo, *ACS Catal.* **2017**, *7*, 3824-3831; e) X. F. Lu, L. Yu, X. W. Lou, *Sci. Adv.* **2019**, *5*, eaav6009; f) Y. Pan, K. Sun, Y. Lin, X. Cao, Y. Cheng, S. Liu, L. Zeng, W.-C. Cheong, D. Zhao, K. Wu, Z. Liu, Y. Liu, D. Wang, Q. Peng, C. Chen, Y. Li, *Nano Energy* **2019**, *56*, 411-419; g) Q. Wang, Z. L. Zhao, S. Dong, D. He, M. J. Lawrence, S. Han, C. Cai, S. Xiang, P. Rodriguez, B. Xiang, Z. Wang, Y. Liang, M. Gu, *Nano Energy* **2018**, *53*, 458-467; h) M. Kim, M. A. R. Anjum, M. Lee, B. J. Lee, J. S. Lee, *Adv. Fun. Mater.* **2019**, *29*, 1809151; i) H. Wang, X. Wang, D. Yang, B. Zheng, Y. Chen, *J. Power Sources* **2018**, *400*, 232-241; j) Z. Chen, R. Wu, Y. Liu, Y. Ha, Y. Guo, D. Sun, M. Liu, F. Fang, *Adv. Mater.* **2018**, *30*, 1802011; k) T. Ouyang, A.-N. Chen, Z.-Z. He, Z.-Q. Liu, Y. Tong, *Chem. Commun.* **2018**, *54*, 9901-9904; l) X. Zhang, X. Yu, L. Zhang, F. Zhou, Y. Liang, R. Wang, *Adv. Fun. Mater.* **2018**, *28*, 1706523; m) M.-Q. Wang, C. Ye, H. Liu, M. Xu, S.-J. Bao, *Angew. Chem. Int. Ed.* **2018**, *57*, 1963-1967.

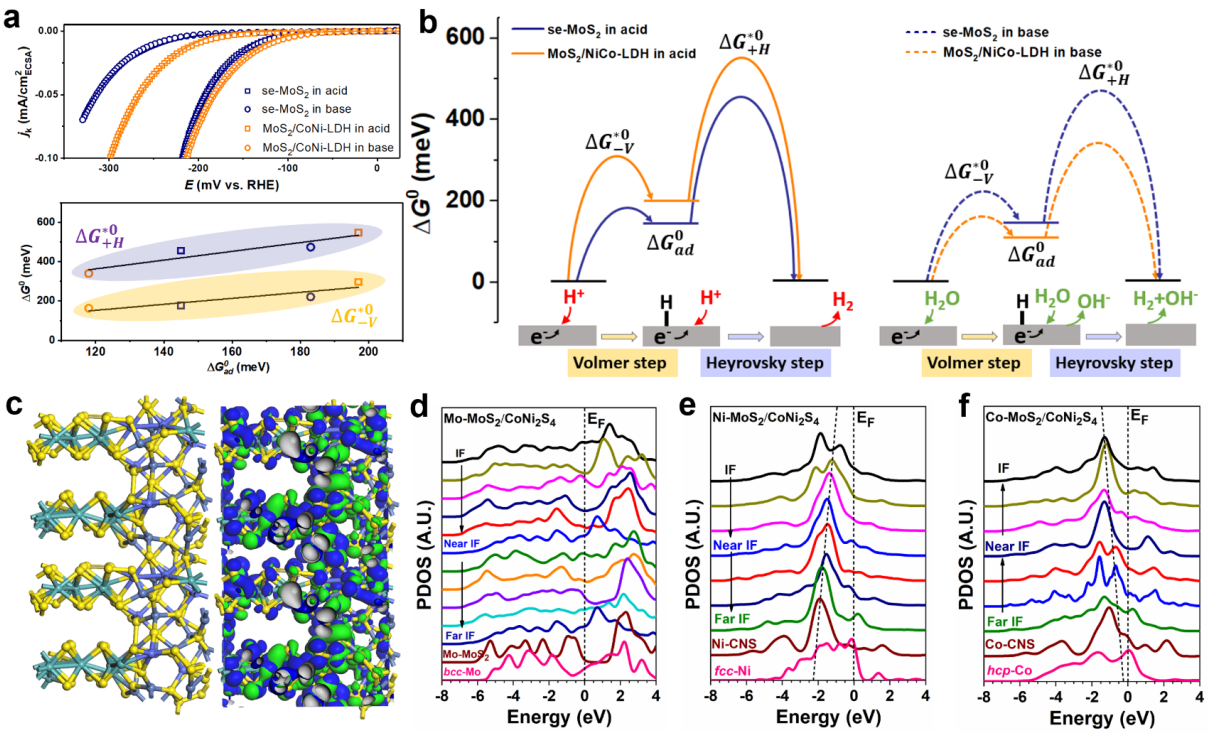

Figure 1. Design of $MoS_2/CoNi_2S_4$ composite for universal HER. (**a**) Kinetic polarization curves for HER performance (up) and fitted linear relationship between the standard free energy of adsorption for the reaction intermediate (ΔG^0_{ad}) and standard activation free energy for Volmer step (ΔG^{*0}_{-V}) and Heyrovsky step (ΔG^{*0}_{+H}) (down) of stepped-edge terminated MoS_2 (se-MoS_2) and MoS_2/NiCo-LDH in both KOH (1 M) and H_2SO_4 (0.5 M) electrolytes. (**b**) Free energy diagram of the dominate Volmer-Heyrovsky pathway of stepped-edge terminated MoS_2 (se-MoS_2) and MoS_2/NiCo-LDH in both KOH (1 M) and H_2SO_4 (0.5 M) electrolytes. (**c**) Side view (left panel) and the real-spatial contour plots for the bonding (blue) and anti-bonding (green) orbitals near the E_F (right panel) of the $MoS_2/CoNi_2S_4$ system. (**d**) The site-dependent PDOSs of Mo from interface (IF) regions towards metal Mo. (**e**) The site-dependent PDOSs of Ni from the interface (IF)` towards metal Ni. CNS represents $CoNi_2S_4$ bulk. (**f**) The site-dependent PDOSs of Co from IF regions towards metal Co.

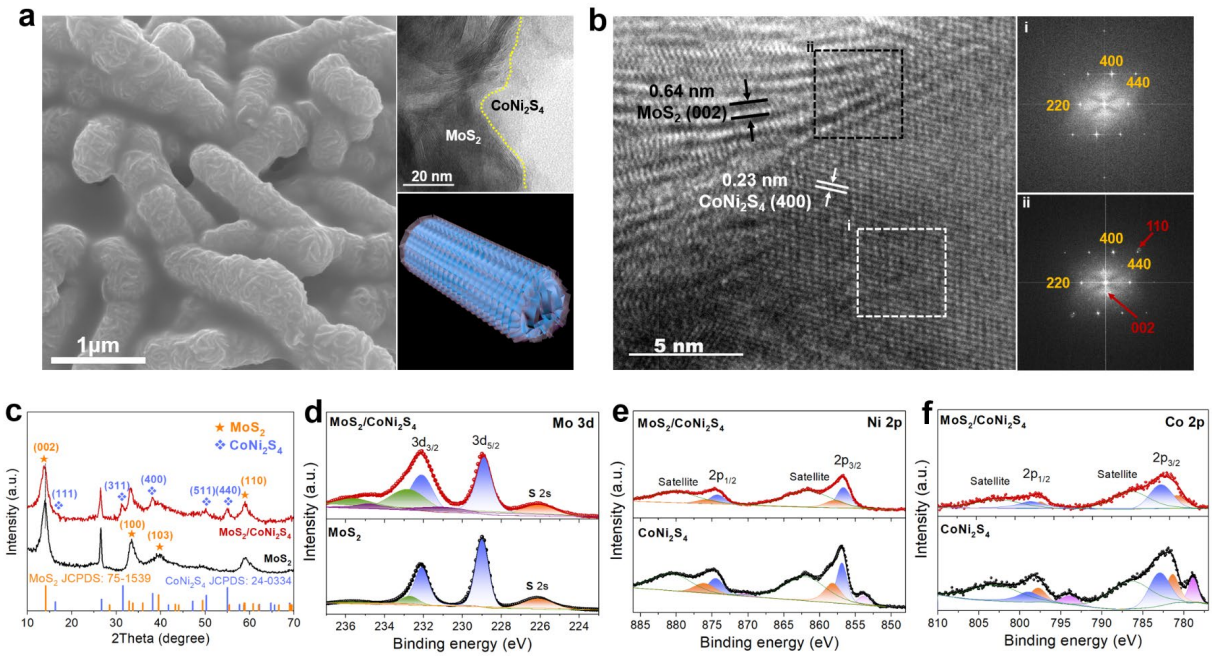

Figure 2. Morphology and structure characterization of $MoS_2/CoNi_2S_4$ composite. (**a**) SEM image of the synthesized $MoS_2/CoNi_2S_4$ composite. Insets are TEM image and schematic illustration of the $MoS_2/CoNi_2S_4$ composite. (**b**) High-resolution TEM image of the $MoS_2/CoNi_2S_4$. Insets are the corresponding fast Fourier transform pattern of the selected areas marked by the dotted square in (**b**). (**c**) Comparison of XRD patterns for the MoS_2 and $MoS_2/CoNi_2S_4$. XPS spectra of (**d**) Mo 3d; (**e**) Ni 2p; and (**f**) Co 2p for bare MoS_2, $CoNi_2S_4$ and $MoS_2/CoNi_2S_4$ composite.

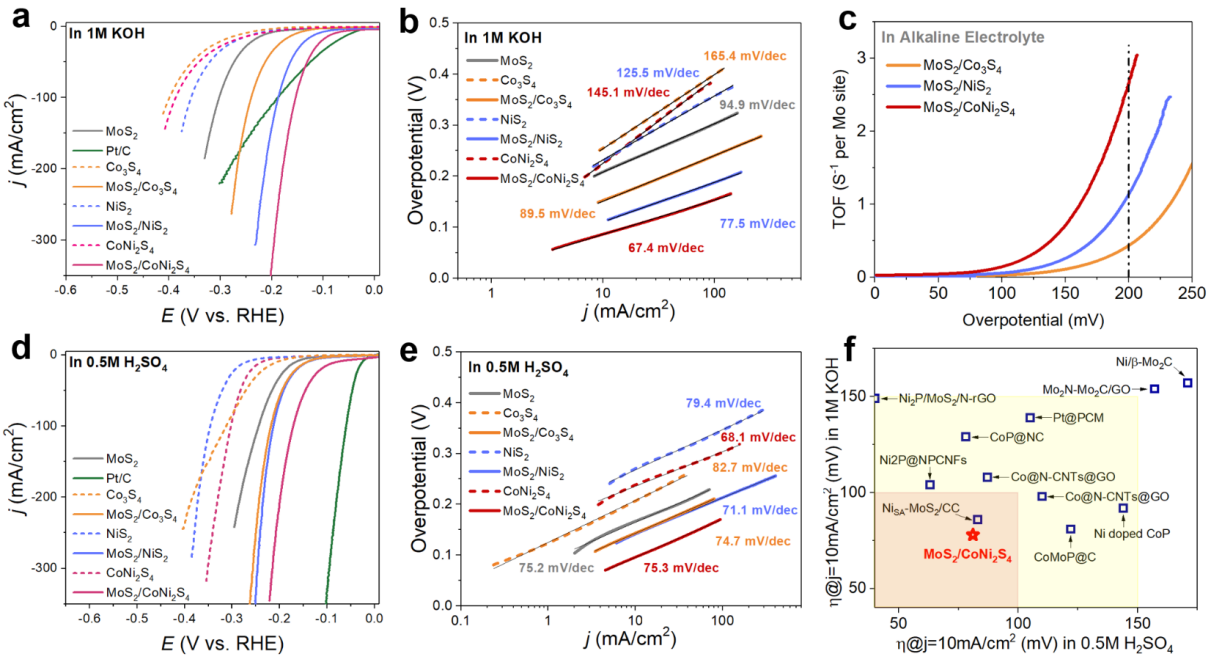

Figure 3. Electrocatalytic performance of $MoS_2/CoNi_2S_4$ catalyst in both base and acid. (**a**.**d**) Polarization curves and (**b**.**e**) corresponding Tafel cures for commercial Pt/C, bare MoS_2, Co_3S_4, NiS_2, $CoNi_2S_4$, and the MoS_2/Co_3S_4, MoS_2/NiS_2, $MoS_2/CoNi_2S_4$ composite catalysts in KOH (1 M) and H_2SO_4 (0.5 M) electrolytes, respectively. (**e**) Turn over frequency (TOF) of MoS_2/Co_3S_4, MoS_2/NiS_2 and $MoS_2/CoNi_2S_4$ composite catalysts in 1 M KOH electrolyte. (f) Comparison of overpotential required to generate a current density of 10 mA/cm^2 on related reported Ni, Co and MoS_2-base compound catalysts in both acidic and alkaline electrolytes.

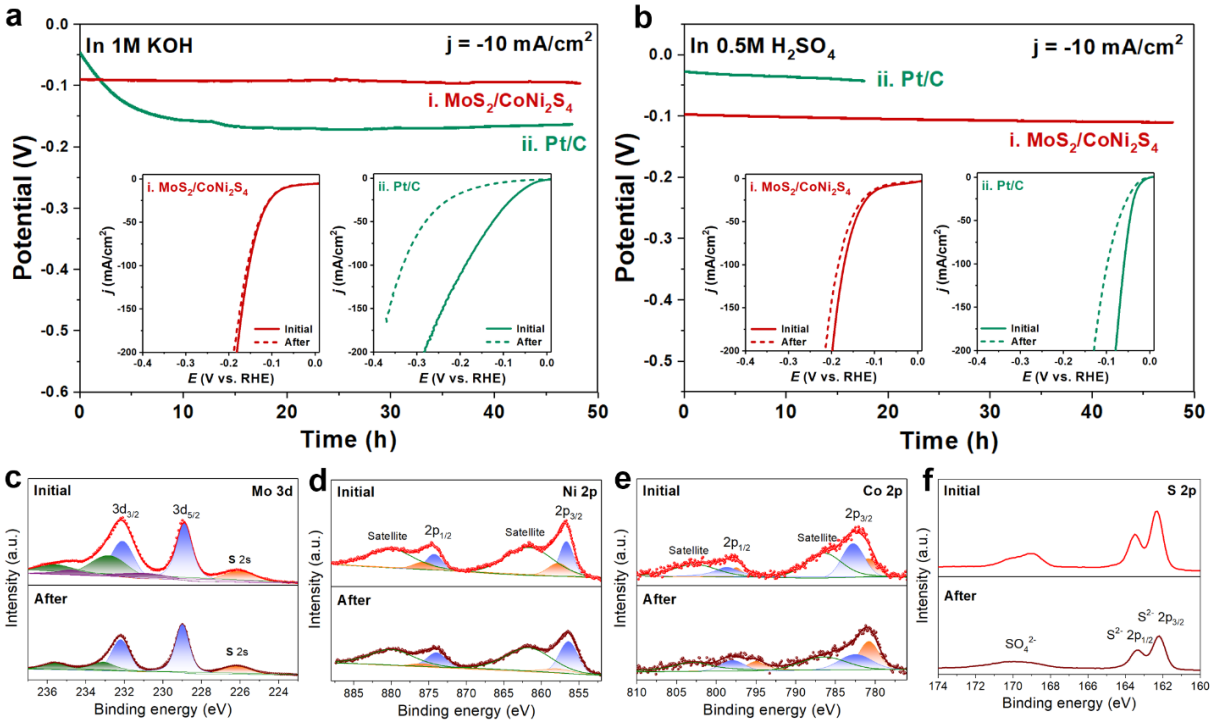

Figure 4. HER stability evaluation of $MoS_2/CoNi_2S_4$ catalyst. Chronoamperometric responses recorded on commercial Pt/C and $MoS_2/CoNi_2S_4$ catalysts in (**a**) 1 M KOH and (**b**) 0.5 M H_2SO_4 solutions. Insets are the polarization curves of ii. $MoS_2/CoNi_2S_4$ and i. commercial Pt/C before and after the durability test. High resolution of XPS (**c**) Mo 3d spectra; (**d**) Ni 2p spectra; (**e**) Co 2p spectra and (**f**) S 2p spectra for $MoS_2/CoNi_2S_4$ composite before and after the chronopotentiometry test in 1 M KOH at -10 mA/cm^2 for 48 hours.

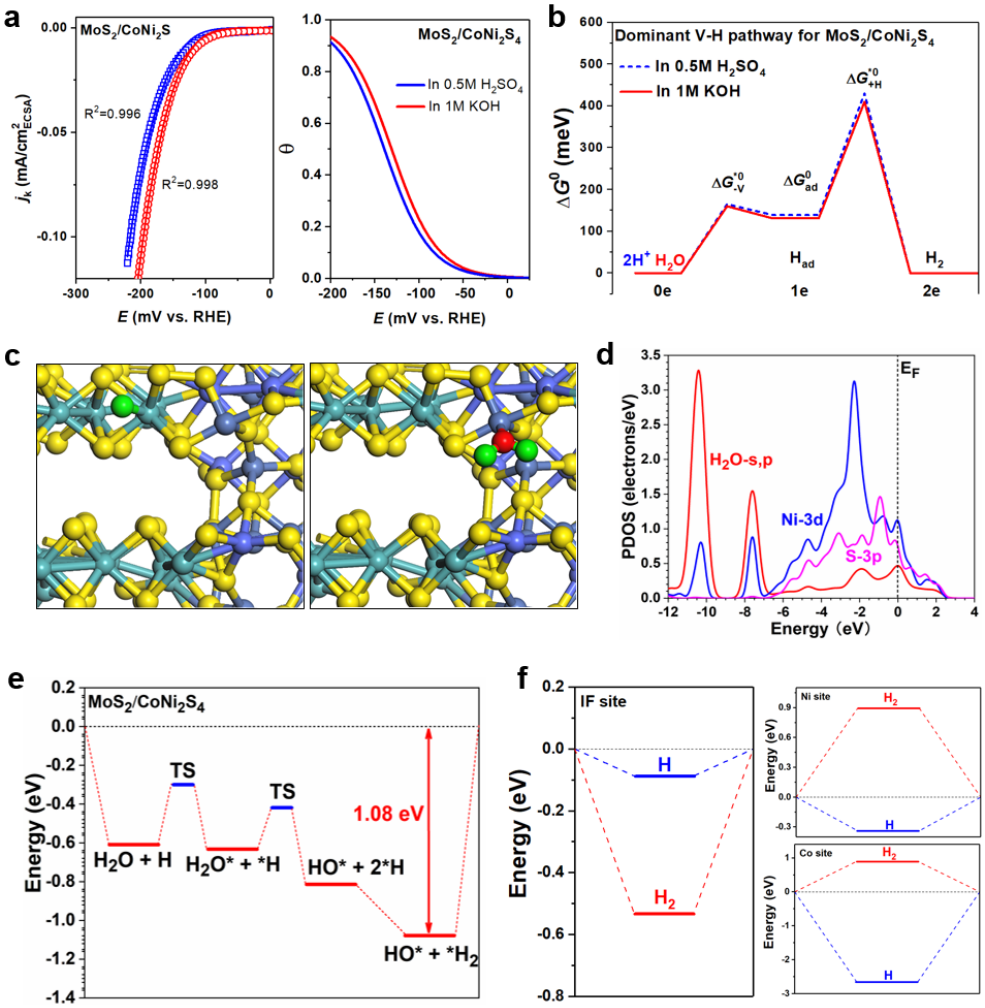

Figure 5. Enhancement mechanism of $MoS_2/CoNi_2S_4$ for universal HER. (**a**) Kinetic current density with the best fitting (left panel) and fractional coverage of Had (right panel) as a function of potential obtained from the dual-pathway kinetic mode fitting for $MoS_2/CoNi_2S_4$ composite in both acid and base. (**b**) Free energy diagram of the $MoS_2/CoNi_2S_4$ composite for HER in both acid and base. (**c**) The local structural configurations for illustrating adsorption of optimal H and H_2O. Red Balls = O, Green Balls= H, Yellow Balls = S, Cyan Balls = Ni, Blue Balls = Co and Olive Balls = Mo. (**d**) The PDOSs comparison of the adsorption of H_2O on the Ni site. (**e**) Free energy pathways for HER under the alkaline condition. (**f**) The formation energies of H and H_2 adsorbed in different sites for $MoS_2/CoNi_2S_4$ system.

The rational design of the interfacial electrocatalyst heterostructure MoS2 guided by the kinetics investigation. By optimizing the electronic structure based on the simultaneous modulation of the 3d-band-offsets of Ni, Co and Mo near the interface, the superior pH-universal hydrogen evolution performances are achieved, which opens new strategy in the design of highly efficient electrocatalysts.

Keyword: Interfacial Electrocatalysis

J. Hu, C. Zhang, P. Yang, M. Sun, J. Xiao, T. Deng, Z. Liu, B. Huang, M. K. H. Leung and S. Yang

Kinetic-oriented construction of MoS_2 synergistic interface to boost pH-universal hydrogen evolution